https://doi.org/10.3311/PPci.25903

Periodica Polytechnica Civil Engineering, 68(4), pp. 1367–1377, 2024

Numerical Procedure for Solving the Nonlinear Behaviour of a Spherical Absorber

Marek Kawulok[1,2*], Martin Čermák[3], Stanislav Pospíšil[1,2], David Juračka[1]

[1] Department of Structural Mechanics, Faculty of Civil Engineering, VSB-Technical University of Ostrava, Ludvíka Podéště 1875/17, 708 00 Ostrava-Poruba, Czech Republic
[2] Institute of Theoretical and Applied Mechanics of the Czech Academy of Sciences, Prosecká 809/76, 190 00 Prague 9, Czech Republic
[3] Department of Mathematics, Faculty of Civil Engineering, VSB-Technical University of Ostrava, Ludvíka Podéště 1875/17, 708 00 Ostrava-Poruba, Czech Republic
* Corresponding author, e-mail: marek.kawulok@vsb.cz

Received: 10 January 2024, Accepted: 27 May 2024, Published online: 22 July 2024

Abstract

The aim of the paper is to perform numerical simulations for a system of nonlinear differential equations that describe the behaviour of a spherical absorber placed in a support bowl and to describe the applied techniques. The motion of the sphere is constrained to a plane problem. The derived system of equations is numerically solved using the continuation method and the modified secant method. The absorber's response to different harmonic excitation forces is simulated to demonstrate the applicability of these techniques in its analysis. The dependence of the response amplitude on the angular frequency of excitation is presented graphically. The results also include a response stability analysis using the Routh-Hurwitz criteria.

Keywords

nonlinear dynamic, modified secant method, continuation method, ball vibration absorber, bifurcation portraits

1 Introduction

Vibrations often have an adverse effect on load-bearing systems of buildings. They may be caused by both human activities, see [1], and natural processes. For example, tall structures (chimneys, radio masts, and towers) and long structures (bridges, footbridges) may experience vibrations due to wind buffeting and aerodynamic instabilities such as galloping, flutter, buffeting, or vortex shedding, as detailed in references [2, 3].

To minimise the effects of vibration and reduce possible damage, damping devices are often incorporated into structures [4]. The most durable and commonly employed are known as passive absorbers, with the ball vibration damper being a notable example from this category. Such a device consists of a supporting bowl and an inner ball. The advantages of this type of absorber are its relatively small size, wide range of possible frequency tuning and minimal maintenance requirements, respectively. There exist examples where this device has been incorporated into wind turbines [5] or in broadcast towers [6]. However, despite its numerous benefits, the absorber may encounter issues with motion instability and problems related to auto-parametric oscillations [7]. The response of the absorber and its efficiency can also be affected by the surface treatment of the support bowl; see [8] for an example. Additionally, the integration of the absorber into the load-bearing system results in a substantial alteration of its mechanical characteristics, necessitating a re-evaluation of the response of the structure, as indicated in [9].

The purpose of this work is to outline a method for the numerical analysis of a set of nonlinear equations that model the behaviour of a spherical absorber situated in a supporting bowl, with a focus solely on planar dynamics. The formulation of these equations is based upon the methodologies outlined in [7]. The solution to these equations employs the Modified Secant Method, see e.g. [10, 11] alongside the Continuation Method as presented in [12, 13]. The history of these methods dates back several decades (see [14, 15, 16]) and its principles are still used today. Among the indisputable advantages of the methods is the possibility of numerically solving multivalued functions.

Cite this article as: Kawulok, M., Čermák, M., Pospíšil, S., Juračka, D. "Numerical Procedure for Solving the Nonlinear Behaviour of a Spherical Absorber", Periodica Polytechnica Civil Engineering, 68(4), pp. 1367–1377, 2024. https://doi.org/10.3311/PPci.25903

However, the procedure also has its drawbacks. For example, due to a poor choice of initial estimates, the computation may not converge. Another disadvantage arises from the nature of the Continuation method, i.e., the fact that we are constantly following a single curve. If there are outlying branches of the solution, a thorough scan through the space of variables is needed to detect them.

Despite these limitations, these techniques were selected to generate curves that illustrate the relationship between the absorber response and the angular frequency of excitation. The absorber's nonlinear characteristics lead to a softening effect, see [17], in these curves, causing them to exhibit multiple response solutions for a given excitation angular frequency. In such instances, it becomes crucial to determine the stability of these solutions, assessing whether they are stable or unstable. The Routh-Hurwitz (R-H) criteria [18] are used to verify the stability of the steady-state response solution. A Routh matrix is calculated for each solution, with an examination of the sign changes in the matrix's first column. If the analysis shows that all terms in this column have the same sign, the solution is considered stable, otherwise it is an unstable solution.

Numerical simulations are carried out for three values of the excitation force amplitude. For each of these cases, the dependence curves between response and excitation angular frequency are plotted. The graphs also contain information about the stability of the solution.

2 Derivation of the system of governing equations

The absorber is limited to planar behaviour only. The principles of derivation and procedures are adopted from the work of [7]. A sketch of the absorber is shown in Fig. 1, where the displacement component $u(t)$ and the angle $\varphi(t)$ describe the motion of the ball. The source of the external excitation is the time-dependent force $F(t)$. Time derivatives are indicated throughout the paper by a point above the corresponding quantity. The time-independent parameters that describe the absorber include the mass of the sphere m, the radius of the sphere r, the mass of the support structure M, the radius of curvature of the support bowl R, and the stiffness K.

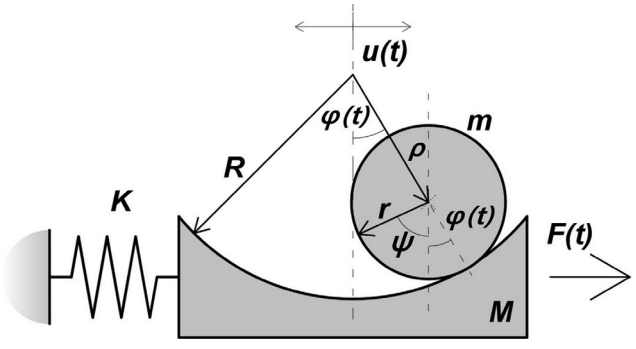

Fig. 1 Schematic drawing of the analysed ball absorber.

Based on the geometry illustrated in Fig. 1, one can deduce the following equations as the kinematic constraints governing the motion:

$$\rho = R - r, \tag{1}$$

$$R\varphi = r\psi + r\varphi, \tag{2a}$$

$$r\psi = R\varphi - r\varphi, \tag{2b}$$

$$\rho\varphi = r\psi. \tag{2c}$$

Eq. (1) determines the radius of movement of the centre of the ball, thus eliminating the possibility of the ball separating from the support bowl. The constraint kinematic conditions summarized in Eq. (2) represent the assumption that the ball continues to roll without any slippage on the bowl's surface, ensuring the rolling motion is preserved. In this equation, ψ is the angle that tracks the rotation of the sphere during rolling motion. Although there are four conditions in total, only two are independent. The Eq. (2c) can be obtained by rearranging the Eq. (2a) when applying Eq. (1).

During the ball's rolling movement and the support structure's oscillation, energy dissipation takes place, a process modelled by damping functions denoted as C. In the scenario under investigation, this damping is accounted for in the analysis through the application of the Rayleigh damping function [19], as described by the equation:

$$C = 0.5\left(m\rho^2 c_\varphi \dot{\varphi}^2 + M c_u \dot{u}^2\right), \tag{3}$$

where C_φ and C_u are the damping coefficients for each motion component. The excitation of the system is provided by a periodic force with the amplitude F_0 and the excitation frequency ω determined by the function:

$$F = F_0 \sin(\omega t). \tag{4}$$

Applying the boundary conditions, excitation function and Rayleigh damping, a system of nonlinear governing differential equations is derived by using the second order Lagrange equation. This system is represented by the following equations:

$$\frac{7}{5}\ddot{\varphi} = c_\varphi \dot{\varphi} + \omega_m^2 \sin\varphi + \frac{\ddot{u}}{\rho}\cos\varphi = 0, \tag{5}$$

$$\eta\ \rho\left(\ddot{\varphi}\cos\varphi-\dot{\varphi}^2\sin\varphi\right)+\ddot{u}\left(1+\eta\right)+\dot{u}c_u+u\ \omega_M^2=\frac{F_0}{M}\sin(\omega t). \tag{6}$$

Where the following substitutions are introduced: $\omega_M^2=K/M$, $\omega_M^2=g/l$ and $\eta=m/M$.

The system of nonlinear, coupled, differential Eqs. (5) and (6) will be further analysed. To further solve the system, it is useful to approximate the sine and cosine functions using the MacLaurin expansion. By considering only the first two terms of an infinite series, cosφ and sinφ can be written as follows:

$$\cos\varphi\approx 1-\frac{1}{2}\varphi^2, \tag{7}$$

$$\sin\varphi\approx\varphi-\frac{1}{6}\varphi^3. \tag{8}$$

The introduction of this substitution leads to a limitation of nonlinearity. The spherical absorber becomes a tuned mass damper that is non-linear spring-supported. The sign before the nonlinear term in Eqs. (7) and (8) also specifies the nature of the resonance curves. Although the numerical method described in the article is able to solve the equations without using this substitution, it is still implemented. Key reasons for doing so include the possibility of using the harmonic balance method and the simplification of further derivations. The effect of the introduced substitution on the accuracy of the solution is a topic that undoubtedly needs to be investigated and will be the subject of future research.

By substituting Eqs. (7) and (8) into Eqs. (5) and (6), the following system of equations is derived:

$$\frac{7}{5}\ddot{\varphi}+c_\varphi\dot{\varphi}+\omega_m^2\left(\varphi-\frac{1}{6}\varphi^3\right)+\frac{\ddot{u}}{\rho}\left(1-\frac{1}{2}\varphi^2\right)=0, \tag{9}$$

$$\eta\ \rho\left[\ddot{\varphi}\left(1-\frac{1}{2}\varphi^2\right)\dot{\varphi}^2\left(\varphi-\frac{1}{6}\varphi^3\right)\right]+\ddot{u}\left(1+\eta\right)+\dot{u}c_u+u\ \omega_M^2=\frac{F_0}{M}\sin(\omega t). \tag{10}$$

According to [7], we expect a response in only one mode of oscillation. Thus, the solution assumes the following response to the harmonic excitation:

$$\varphi=\alpha\sin(\omega t)+\beta\cos(\omega t), \tag{11}$$

$$u=\gamma\sin(\omega t)+\delta\cos(\omega t), \tag{12}$$

where $\alpha(t)$, $\beta(t)$, $\gamma(t)$, and $\delta(t)$ are new unknown functions. The validity of the assumptions (11) and (12) is verified by analysing the stability of the solution.

In order to know the velocity components, it is necessary to carry out derivation of Eqs. (11) and (12) with respect to time, leading to the following expressions:

$$\dot{\varphi}=\alpha\ \omega\cos(\omega t)-\beta\ \omega\sin(\omega t)+\dot{\alpha}\sin(\omega t)+\dot{\beta}\cos(\omega t), \tag{13}$$

$$\dot{u}=\gamma\ \omega\cos(\omega t)-\delta\ \omega\sin(\omega t)+\dot{\gamma}\sin(\omega t)+\dot{\delta}\cos(\omega t). \tag{14}$$

The unknown functions are required to comply with Eqs. (9) and (10). However, given that there are four unknown functions, introducing two additional conditions is necessary. These conditions, which the unknown functions must meet, can be selected freely. Yet, their careful formulation is chosen to simplify further derivations. As suggested by references [20, 21], it proves advantageous to specify the conditions in the form presented below:

$$\dot{\alpha}\sin(\omega t)+\dot{\beta}\cos(\omega t)=0, \tag{15}$$

$$\dot{\gamma}\sin(\omega t)+\dot{\delta}\cos(\omega t)=0. \tag{16}$$

Introducing the new constraints by means of Eqs. (15) and (16) also guarantees that the new variables span the original space.

Observing Eqs. (13) and (14), it can be noticed that the sum of the last two terms containing the derivative of the unknown functions $\dot{\alpha}$, $\dot{\beta}$, $\dot{\gamma}$, $\dot{\delta}$ becomes zero following the implementation of the additional conditions outlined in Eqs. (15) and (16). By excluding these last two terms, these equations can be reformulated as follows:

$$\dot{\varphi}=\alpha\ \omega\cos(\omega t)-\beta\ \omega\sin(\omega t), \tag{17}$$

$$\dot{u}=\gamma\ \omega\cos(\omega t)-\delta\ \omega\sin(\omega t). \tag{18}$$

Since system of Eqs. (9) and (10) also contain acceleration components, the assumed solution has to be differentiated again, resulting in the following equations:

$$\ddot{\varphi}=\dot{\alpha}\ \omega\cos(\omega t)-\alpha\ \omega^2\sin(\omega t)-\dot{\beta}\ \omega\sin(\omega t)-\beta\ \omega^2\cos(\omega t), \tag{19}$$

$$\ddot{u}=\dot{\gamma}\ \omega\cos(\omega t)-\gamma\ \omega^2\sin(\omega t)-\dot{\delta}\ \omega\sin(\omega t)-\delta\ \omega^2\cos(\omega t). \tag{20}$$

It is important to note that the specific selection of differential conditions defined by Eqs. (15) and (16) allows for the simplification of expressions for $\ddot{\varphi}$, $\ddot{u}$, resulting in the

presence of only the first derivatives of the new variables $\alpha, \beta, \gamma, \delta$ in the transformed system. Further details can be found, for example, in [22].

The next step of the solution is to substitute the assumed solution (Eqs. (11) and (12)), the first derivative (Eqs. (17) and (18)) and the second derivative (Eqs. (19) and (20)) into the system of governing Eqs. (9) and (10). These equations can be further modified by using trigonometric identities.

All the modifications made enable the solution of the equations of motion using the harmonic balance method, which is used to calculate the steady-state response of nonlinear differential equations. Using only a few harmonic terms, it is possible to attain satisfactory accuracy, a fact underscored by the comparison of the harmonic balance method with the numerical integration method for solving the Duffing equation, as presented in [23]. For the analysed absorber, only the first harmonic terms are retained. For each of the original equations, the coefficients that multiply the sine and the coefficients that multiply the cosine are listed. This results in four equations containing $\alpha, \beta, \gamma, \delta$ and their derivatives $\dot{\alpha}, \dot{\beta}, \dot{\gamma}, \dot{\delta}$. Since we consider only stationary solutions, the derivatives $\dot{\alpha}, \dot{\beta}, \dot{\gamma}, \dot{\delta}$ are zero. The equation system can be written as:

$$\boldsymbol{f}(\alpha,\beta,\gamma,\delta)=\begin{pmatrix} f_1(\alpha,\beta,\gamma,\delta) \\ f_2(\alpha,\beta,\gamma,\delta) \\ f_3(\alpha,\beta,\gamma,\delta) \\ f_4(\alpha,\beta,\gamma,\delta) \end{pmatrix}=\mathbf{0}. \tag{21}$$

In Eq. (21) are f_1, f_2, f_3, f_4 functions of $\alpha, \beta, \gamma, \delta$ and can be written in as follows:

$$f_1=\frac{1}{40\rho}\begin{bmatrix} -5\alpha^3\ \rho\omega_m^2+15\alpha^2\gamma\omega^2 \\ +\alpha\left(-5\rho\omega_m^2\beta^2+10\omega^2\beta\delta-56\rho\omega^2+40\omega_m^2\rho\right) \\ +5\beta^2\gamma\omega^2-40\beta c_\varphi\omega\rho-40\gamma\omega^2 \end{bmatrix}, \tag{22}$$

$$f_2=\frac{1}{40\rho}\begin{bmatrix} -5\beta^3\rho\omega_m^2+15\beta^2\delta\omega^2 \\ +\beta\left(-5\rho\omega_m^2\alpha^2+10\omega^2\alpha\gamma-56p\omega^2+40\omega_m^2\rho\right) \\ +5\alpha^2\delta\omega^2+40\alpha c_\varphi\omega\rho-40\delta\omega^2 \end{bmatrix}, \tag{23}$$

$$f_3=\frac{1}{48M}\begin{bmatrix} M\beta^5\eta\omega^2\rho+2M\eta\rho\omega^2\beta^3\left(\alpha^2+3\right) \\ +M\eta\rho\omega^2\beta\left(\alpha^4+6\alpha^2-48\right) \\ +48M\gamma c_u\omega-48\delta M\left(\eta+1\right)\omega^2-\omega_M^2 \end{bmatrix}, \tag{24}$$

$$f_4=\frac{1}{48M}\begin{bmatrix} M\alpha^5\eta\omega^2\rho+2M\eta\rho\omega^2\alpha^3\left(\beta^2+3\right) \\ +M\eta\rho\omega^2\alpha\left(\beta^4+6\beta^2-48\right)-48M\delta c_u\omega \\ -48\gamma M\left(\left(\eta+1\right)\omega^2-\omega_M^2\right)-48F_0 \end{bmatrix}. \tag{25}$$

The numerical solution of system (21) gives constant values for $\alpha, \beta, \gamma, \delta$. The amplitude P and D of the steady-state response can be determined by these equations:

$$P=\sqrt{\alpha^2+\beta^2}, \tag{26}$$

$$D=\sqrt{\gamma^2+\delta^2}. \tag{27}$$

The validity of the assumed solutions given by Eqs. (11) and (12) must be verified by stability analysis using the Routh-Hurwitz criterion. However, in the case of the steady-state solution the system of equations in the form of Eq. (21) is subject to solution in the case of stability analysis, the complete solution has to be considered. In this case, the system is in the following form:

$$\boldsymbol{N}(\alpha,\beta,\gamma,\delta)\times\dot{\boldsymbol{x}}=\boldsymbol{f}(\alpha,\beta,\gamma,\delta), \tag{28}$$

where $\dot{\boldsymbol{x}}$ is a vector containing $\dot{\alpha}, \dot{\beta}, \dot{\gamma}, \dot{\delta}$ and $\boldsymbol{N}$ is a matrix which can be written as:

$$\boldsymbol{N}=\begin{pmatrix} 0 & \frac{-7\omega}{5} & \frac{-\alpha\beta\omega}{4\rho} & N_{1,4} \\ \frac{-7\omega}{5} & 0 & N_{2,3} & \frac{\alpha\beta\omega}{4\rho} \\ N_{3,1} & \frac{\alpha\beta\eta\omega\rho}{4} & \omega\left(\eta+1\right) & 0 \\ \frac{-\alpha\beta\eta\omega\rho}{4} & N_{4,2} & 0 & -\omega\left(\eta+1\right) \end{pmatrix}, \tag{29}$$

in which the following substitution was made:

$$N_{1,4}=\frac{\omega\left(3\alpha^2+\beta^2-8\right)}{8\rho}, \tag{30}$$

$$N_{2,3}=-\frac{\omega\left(\alpha^2+3\beta^2-8\right)}{8\rho}, \tag{31}$$

$$N_{3,4}=-\frac{\omega\eta\rho\left(\alpha^2+3\beta^2-8\right)}{8}, \tag{32}$$

$$N_{4,2}=\frac{\omega\eta\rho\left(3\alpha^2+\beta^2-8\right)}{8}. \tag{33}$$

By modifying Eq. (28) one obtains the following equation for $\dot{\boldsymbol{x}}$:

$$\dot{\boldsymbol{x}}=\boldsymbol{N}^{-1}\boldsymbol{f}. \tag{34}$$

To analyse stability using R-H conditions, knowledge of the characteristic polynomial is essential. The first step to establish it involves the calculation of the Jacobian matrix $\boldsymbol{A}$ of the right-hand side of Eq. (34), as follows:

$$\boldsymbol{A} = jac\left(\boldsymbol{N}^{-1}\boldsymbol{f}\right). \tag{35}$$

The characteristic polynomial is then given by the equation:

$$det = (\lambda \boldsymbol{I} - \boldsymbol{A}) = 0, \tag{36}$$

where $\boldsymbol{I}$ is the identical matrix. Using the coefficient of λ^4, λ^3, λ^2, λ^1, λ^0 it is possible to construct a Routh table and examine the change of signs in the first column. If all terms in a column have the same sign, the solution is considered stable. However, if there is a sign change between the values in the column, the solution is unstable.

3 Description of the solution procedure using numerical methods

This chapter focuses on detailing the numerical solution of the α, β, γ, δ appearing in Eq. (21). These unknowns will be determined for different values of the excitation frequency in order to generate response curves representing the dependence of the steady-state response amplitudes on the excitation frequency. The response amplitudes are given by Eqs. (26) and (27).

Several procedures can be used to solve the system of equations. One possibility is to use Newton's iterative method, which is suitable for the case when the nonlinear character of the system is negligible, for example for a small amplitude of the excitation force. However, as the amplitudes increase, the influence of nonlinearity can be expected to increase [24]. In this case the classical Newton's method fails and it is necessary to use different methods. The Continuation Method in combination with the Modified Secant Method was chosen for the analysed system. These methods are also capable of numerically capturing cases where, due to the effect of softening behaviour of resonance curves, several values of response amplitudes will belong to one value of excitation angular frequency.

In the case of a ball absorber placed on a supporting bowl, the task is to solve the system of equations given by Eq. (21). In the upcoming explanation of the iterative process, only f_1 will be used. Subscript i represents the current iteration step and $i + 1$ represents the next iteration step. Considering only the linear terms of the multivariable Taylor series we can write:

$$f_{1,i+1} - f_{1,i} = \frac{\partial f_{1,i}}{\partial \alpha}\Delta\alpha + \frac{\partial f_{1,i}}{\partial \beta}\Delta\beta + \frac{\partial f_{1,i}}{\partial \gamma}\Delta\gamma + \frac{\partial f_{1,i}}{\partial \delta}\Delta\delta. \tag{37}$$

The objective of the iterations is to achieve the value $f_{1,i+1}=0$, so we can modify Eq. (38) into the form:

$$f_{1,i} = -\left(\frac{\partial f_{1,i}}{\partial \alpha}\Delta\alpha + \frac{\partial f_{1,i}}{\partial \beta}\Delta\beta + \frac{\partial f_{1,i}}{\partial \gamma}\Delta\gamma + \frac{\partial f_{1,i}}{\partial \delta}\Delta\delta\right). \tag{38}$$

For the terms $\Delta\alpha$, $\Delta\beta$, $\Delta\gamma$, and $\Delta\delta$ holds:

$$\Delta\alpha = \alpha_{i+1} - \alpha_i \rightarrow \alpha_{i+1} = \alpha_i + \Delta\alpha, \tag{39}$$

$$\Delta\beta = \beta_{i+1} - \beta_i \rightarrow \beta_{i+1} = \beta_i + \Delta\beta, \tag{40}$$

$$\Delta\gamma = \gamma_{i+1} - \gamma_i \rightarrow \gamma_{i+1} = \gamma_i + \Delta\gamma, \tag{41}$$

$$\Delta\delta = \delta_{i+1} - \delta_i \rightarrow \delta_{i+1} = \delta_i + \Delta\delta. \tag{42}$$

Performing the modification according to Eq. (38) for all equations, we obtain:

$$\begin{pmatrix} f_{1,i} \\ f_{2,i} \\ f_{3,i} \\ f_{4,i} \end{pmatrix} = -\begin{pmatrix} \frac{\partial f_{1,i}}{\partial \alpha} & \frac{\partial f_{1,i}}{\partial \beta} & \frac{\partial f_{1,i}}{\partial \gamma} & \frac{\partial f_{1,i}}{\partial \delta} \\ \frac{\partial f_{2,i}}{\partial \alpha} & \frac{\partial f_{2,i}}{\partial \beta} & \frac{\partial f_{2,i}}{\partial \gamma} & \frac{\partial f_{2,i}}{\partial \delta} \\ \frac{\partial f_{3,i}}{\partial \alpha} & \frac{\partial f_{3,i}}{\partial \beta} & \frac{\partial f_{3,i}}{\partial \gamma} & \frac{\partial f_{3,i}}{\partial \delta} \\ \frac{\partial f_{4,i}}{\partial \alpha} & \frac{\partial f_{4,i}}{\partial \beta} & \frac{\partial f_{4,i}}{\partial \gamma} & \frac{\partial f_{4,i}}{\partial \delta} \end{pmatrix} \times \begin{pmatrix} \Delta\alpha \\ \Delta\beta \\ \Delta\gamma \\ \Delta\delta \end{pmatrix}, \tag{43}$$

where the matrix composed of partial derivatives is known as the Jacobi matrix $\boldsymbol{J}$. To construct this matrix numerically, the Modified Secant Method is employed. This approach utilizes the finite difference approximation for derivatives, relying on selecting a small, arbitrary deviation ξ from the initial value. The formulas for calculating the partial derivatives by this method are given, for example, for the two terms in Eq. (43) as:

$$\frac{\partial f_1}{\partial \alpha} \approx \frac{f_1(\alpha+\xi,\beta,\gamma,\delta) - f_1(\alpha,\beta,\gamma,\delta)}{\xi}, \tag{44}$$

$$\frac{\partial f_4}{\partial \gamma} \approx \frac{f_4(\alpha,\beta,\gamma+\xi,\delta) - f_4(\alpha,\beta,\gamma,\delta)}{\xi}. \tag{45}$$

In this manner, the entire Jacobi matrix can be constructed. To solve for the unknowns in Eq. (43), it is necessary to construct the inverse of the Jacobian matrix $\boldsymbol{J}^{-1}$.

Afterwards, the solution of Eq. (43) can be written as follows:

$$\begin{pmatrix} \Delta\alpha \\ \Delta\beta \\ \Delta\gamma \\ \Delta\delta \end{pmatrix} = -\boldsymbol{J}^{-1}.\begin{pmatrix} f_{1,i} \\ f_{2,i} \\ f_{3,i} \\ f_{4,i} \end{pmatrix}. \tag{46}$$

The resulting values for $\Delta\alpha$, $\Delta\beta$, $\Delta\gamma$, $\Delta\delta$ are added to the values of α_i, β_i, γ_i, δ_i according to Eqs. (39), (40), (41), and (42) to obtain the value of the unknowns for the next iterative step α_{i+1}, β_{i+1}, γ_{i+1}, and δ_{i+1}. To begin the iterative process, it is necessary first to determine an initial estimate of the quantities. The iteration loop is terminated when the acceptable error threshold e is reached. The value of the error threshold e is specified by the user and the accuracy of the calculation is defined as the Euclidean norm:

$$\left\|f_e\right\| = \sqrt{f_1^2 + f_2^2 + f_3^2 + f_4^2}. \tag{47}$$

Hence, to terminate an iteration, the following must hold:

$$\left\|f_e\right\| < e. \tag{48}$$

The described Modified Secant Method will be used to calculate the values of the unknowns in each step and to ensure the proper functioning of the continuation method.

The Continuation Method is effective and facilitates the solving of multivalued functions. This capability enables the mapping of the relationship between amplitude and angular excitation frequency, even in the presence of the softening effect, where the resonance curves cease to behave as a conventional function. In such cases, a single value of excitation angular frequency may correspond to more than one distinct value of response amplitude. To construct curves utilizing this method, it's necessary to have knowledge of two initial points on the curve. Creation of the curves using this method requires knowledge of the two initial points on that curve. In the case of a ball absorber one may select two values of the excitation frequency (ω_1 and ω_2) and proceed with an initial estimation of all four unknowns at both points ($\alpha_{1,0}$, $\beta_{1,0}$, $\gamma_{1,0}$, $\delta_{1,0}$ for the first point and $\alpha_{2,0}$, $\beta_{2,0}$, $\gamma_{2,0}$, $\delta_{2,0}$ the second one). In the vector form, we can write these guesses $\boldsymbol{v}_{\mathbf{1,0}}$ and $\boldsymbol{v}_{\mathbf{2,0}}$ as follows:

$$v_{\mathbf{1,0}} = \begin{pmatrix} \alpha_{\mathbf{1,0}} \\ \beta_{\mathbf{1,0}} \\ \gamma_{\mathbf{1,0}} \\ \delta_{\mathbf{1,0}} \\ \omega_{\mathbf{1}} \end{pmatrix};\ v_{\mathbf{2,0}} = \begin{pmatrix} \alpha_{\mathbf{2,0}} \\ \beta_{\mathbf{2,0}} \\ \gamma_{\mathbf{2,0}} \\ \delta_{\mathbf{2,0}} \\ \omega_{\mathbf{2}} \end{pmatrix}. \tag{49}$$

The results of solving Eq. (21) for these two points can be written together with the corresponding value of ω in the form of vectors:

$$\boldsymbol{v}_{\mathbf{1}} = \begin{pmatrix} \alpha_{\mathbf{1}} \\ \beta_{\mathbf{1}} \\ \gamma_{\mathbf{1}} \\ \delta_{\mathbf{1}} \\ \omega_{\mathbf{1}} \end{pmatrix};\ \boldsymbol{v}_{\mathbf{2}} = \begin{pmatrix} \alpha_{\mathbf{2}} \\ \beta_{\mathbf{2}} \\ \gamma_{\mathbf{2}} \\ \delta_{\mathbf{2}} \\ \omega_{\mathbf{2}} \end{pmatrix}. \tag{50}$$

Another critical parameter is the length of the curve segment, or the distance along the curve between the two points that need to be determined. This length S is constant for the entire calculation and is determined as the norm of the difference of vectors Eq. (50). The calculation is therefore given by equation:

$$S = \left\|\boldsymbol{v}_{\mathbf{2}} - \boldsymbol{v}_{\mathbf{1}}\right\|. \tag{51}$$

The size of the vector $\boldsymbol{v}$ entries in Eq. (51) may vary and depend on the units used, which may lead to scaling prior to norm evaluation. If this were ignored, the forward step procedure would have different apparent rates in different directions of the parameter space. With this information, one can move forward with calculating subsequent points. The initial estimate for the j-th point can typically be expressed as:

$$\boldsymbol{vj}, \mathbf{0} = 2 \times \boldsymbol{v}_{\boldsymbol{j-1}} - \boldsymbol{v}_{\boldsymbol{j-2}}, \tag{52}$$

where $\boldsymbol{v}_{\boldsymbol{j-1}}$ is a vector of result values of the previous point, $\boldsymbol{v}_{\boldsymbol{j-2}}$ is a vector of result values from the point preceding $\boldsymbol{v}_{\boldsymbol{j-1}}$ and $\boldsymbol{v}_{\boldsymbol{j,0}}$ is a vector of the following form:

$$\boldsymbol{v}_{\boldsymbol{j,0}} = \begin{pmatrix} \alpha_{\boldsymbol{j,0}} \\ \beta_{\boldsymbol{j,0}} \\ \gamma_{\boldsymbol{j,0}} \\ \delta_{\boldsymbol{j,0}} \\ \omega_{\boldsymbol{j,0}} \end{pmatrix}. \tag{53}$$

Contrary to the first two points, where the angular excitation frequency value was set, in subsequent calculations, this value will vary. This variation is due to the condition that the curve distance S remains consistent among all computed points. This condition is formalized by the equation:

$$\left\|\boldsymbol{v}_j - \boldsymbol{v}_{j-1}\right\| - S = 0. \tag{54}$$

The Eq. (21), which were solved for the first two points, are replaced for the rest of the calculation by the following system of equations:

$$\begin{aligned} f_1\left(\alpha_j,\beta_j,\gamma_j,\delta_j,\omega_j\right)&=0,\\ f_2\left(\alpha_j,\beta_j,\gamma_j,\delta_j,\omega_j\right)&=0,\\ f_3\left(\alpha_j,\beta_j,\gamma_j,\delta_j,\omega_j\right)&=0,\\ f_4\left(\alpha_j,\beta_j,\gamma_j,\delta_j,\omega_j\right)&=0,\\ \left\|\boldsymbol{v}_j-\boldsymbol{v}_{j-1}\right\|-S&=0. \end{aligned} \tag{55}$$

Also, this system of equations is solved using the Modified Secant Method described above. During the calculation, the resulting values are substituted into the derived Routh table. Subsequently, it is checked whether there is a change of sign in the values of the first column of this table. If there is no change and all members are either positive or negative, the solution is stable. However, if at least one change in sign is observed the solution is considered as unstable.

4 Numerical simulations and results

The subsequent portion of this paper concentrates on the numerical simulation of the equations formulated in Section 2, utilizing the methodologies and strategies described in Section 3. The MATLAB [25] software, specifically its built-in "*mldivide*" algorithm for resolving the system of equations, was employed to develop and conduct the calculations [26]. This function was used to solve Eq. (46) in an iterative calculation using the Modified Secant Method for each step of the Continuation Method.

The values of the characteristics that describe the example absorber are given in Table 1.

The principal outcome of the simulations is the curves depicting the relationship between the excitation angular frequency ω and the amplitudes as detailed by Eqs. (26) and (37). For the purpose of plotting, an angular excitation frequency range of 2–5 rad s^{-1} was selected. In order to observe the occurrence of unstable parts of the solution, the graphs are plotted for several amplitudes of the excitation force F_0 = 2.5, 3.5 and 6 N. These values were deliberately chosen to demonstrate the formation of unstable regions.

Once the parameters of the system are defined, the subsequent steps involve establishing initial guesses of the unknowns within the first two steps of the Continuation Method. Additionally, it's essential to specify the excitation angular frequencies corresponding to these points.

Table 1 Absorber parameters

Parameter name	Symbol	Value
Mass of the bowl	M	9 kg
Bowl radius of curvature	R	1.1 m
Mass of the ball	m	3 kg
Radius of the ball	r	0.3 m
Spring stiffness	K	150 N m^{-1}
Damping coefficient	c_φ	0.12
Damping coefficient	c_u	0.18

Since these two points are used to calculate the step length on the curve S, see. Eq. (51), the choice of the distance between ω_1 and ω_2 is crucial for the number of calculation points. A smaller difference between these two values leads to more points on the curve. All values of the initial parameter values are defined in Table 2.

The first simulations were performed with the value of the excitation force amplitude F_0 = 2.5 N. Resulting graphs can be seen in Figs. 2 and 3, showing the response amplitudes. One can observe two regions of excitation angular frequencies where the local maximum of amplitudes is found. For the response P, the maximum values are achieved at the $\omega_{max,1}$ = 2.647 rad s^{-1} and $\omega_{max,2}$ =4.235 rad s^{-1}. For the response D then, at $\omega_{max,1}$ =2.641 rad s^{-1} and $\omega_{max,2}$ =4.239 rad s^{-1}. The stability analysis, conducted via R-H (Routh-Hurwitz) conditions, did not expose any unstable solutions; this outcome is typically represented by a solid line, signifying a stable solution.

In the following simulation, the amplitude of the excitation force F_0 was increased to 3.5 N. The effect of amplitude increase can be observed in both Figs. 4 and 5. The excitation angular frequency at which the maximum response is

Table 2 Parameter estimation for the first two steps of the Continuation Method

Number of the j-th point	1	2
Initial estimate of $\alpha_{j,0}$ (rad)	0	0
Initial estimate of $\beta_{j,0}$ (rad)	0	0
Initial estimate of $\gamma_{j,0}$ (m)	0	0
Initial estimate of $\delta_{j,0}$ (m)	0	0
Excitation angular frequency $\omega_{j,0}$ (rad s^{-1})	2.000	2.001

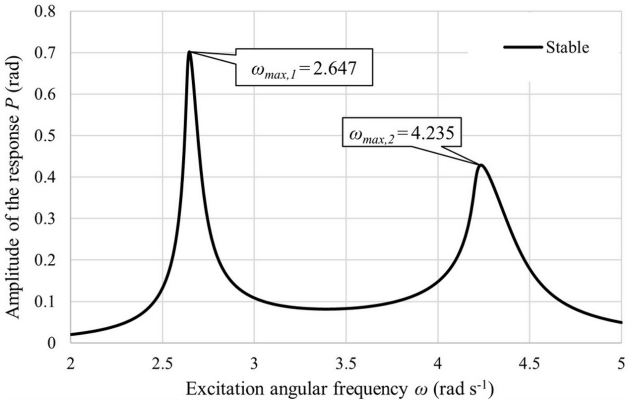

Fig. 2 Curve of response amplitude P versus excitation angular frequency . The absorber system is excited by a periodic force with amplitude N. The boxed values indicate the value of for which the maximum response was achieved

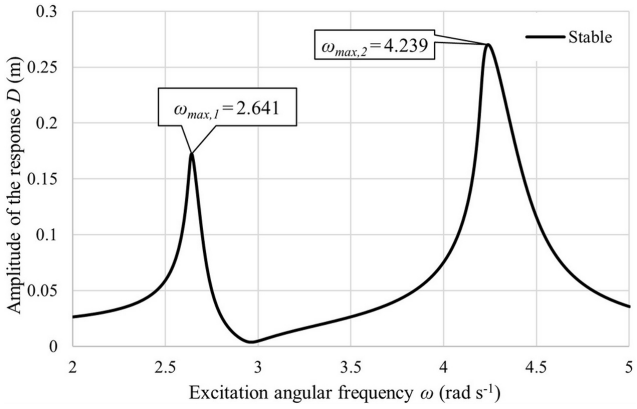

Fig. 3 Curve of response amplitude D versus excitation angular frequency . The absorber system is excited by a periodic force with amplitude N. The boxed values indicate the value of for which the maximum response was achieved

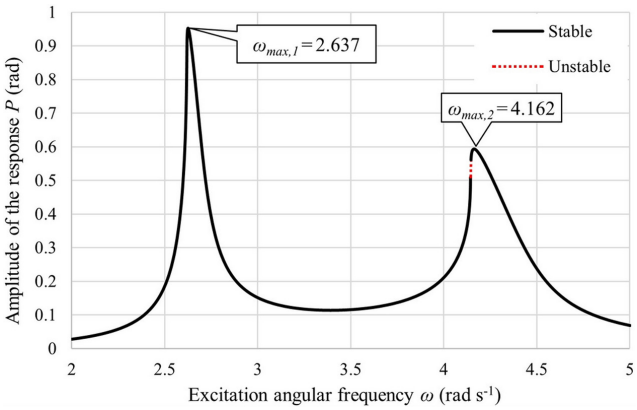

Fig. 4 Curve of response amplitude P versus excitation angular frequency . The absorber system is excited by a periodic force with amplitude N. The boxed values indicate the value of for which the maximum response was achieved. Unstable solutions are found in the area between rad s-1 and rad s-1

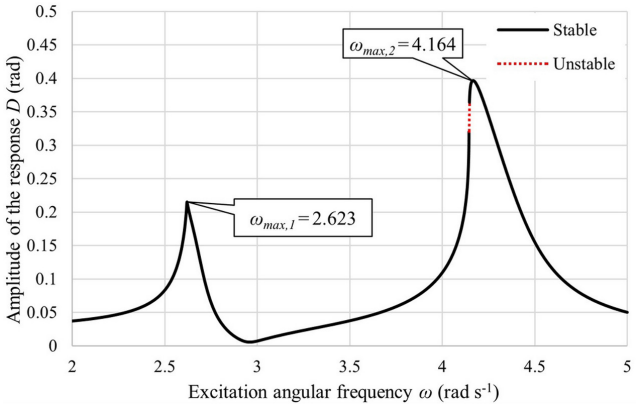

Fig. 5 Curve of response amplitude D versus excitation angular frequency . The absorber system is excited by a periodic force with amplitude N. The boxed values indicate the value of for which the maximum response was achieved. Unstable solutions are found in the area between rad s-1 and rad s-1

achieved undergoes a shift in both resonance curves. Now for the response component P the maxima are reached at $\omega_{max,1} = 2.637$ rad s^{-1}, $\omega_{max,2} = 4.162$ rad s^{-1} and for the response component D at $\omega_{max,1}$ = 2.623 rad s^{-1} and $\omega_{max,2}$ = 4.164 rad s^{-1}. In the region of the second peak, a softening effect is becoming apparent. Higher force amplitude also results in the appearance of an unstable solution. Using R-H conditions, unstable solutions were detected in the ranges from ω = 4.145 rad s^{-1} to ω = 4.146 rad s^{-1}. This unstable part of the solution is indicated by the red dotted line in Figs 4 and 5.

The last simulations are performed with the value of the excitation force amplitude F_0 = 6 N. The simulation results show two unstable regions around the first and second maximum response of both components (Figs. 6 and 7).

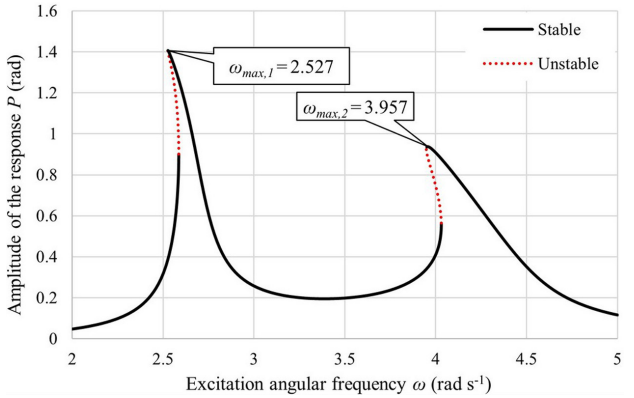

Fig. 6 Curve of response amplitude P versus excitation angular frequency . The absorber system is excited by a periodic force with amplitude N. The boxed values indicate the value of for which the maximum response was achieved. The first region of the unstable solution is located between rad s-1 and rad s-1 The second region is between and rad s-1

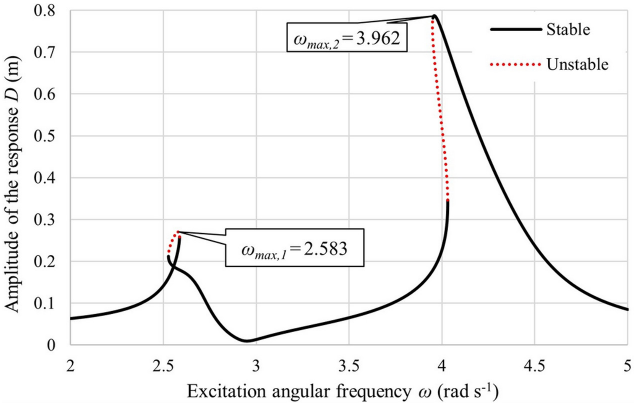

Fig. 7 Curve of response amplitude D versus excitation angular frequency . The absorber system is excited by a periodic force with amplitude N. The boxed values indicate the value of for which the maximum response was achieved. The first region of the unstable solution is located between rad s-1 and rad s-1 The second region is between and rad s-1

Stability analysis of the steady-state solution revealed the presence of two unstable regions. The first region lies between values $\omega = 2.527$ rad s^{-1} and $\omega = 2.587$ rad s^{-1} and the second between $\omega = 3.951$ rad s^{-1} and $\omega = 4.031$ rad s^{-1}. The location of the unstable solutions is indicated by the red dotted line. In the graph showing the dependence between the response component P and the angular excitation frequency (Fig. 6), we can observe a softening effect in the region of both local response maxima. The graph for the response component D (Fig. 7) shows this effect only in the region of the second local maxima. Compared to the previous simulation for $F_0 = 3.5$ N, there is a shift of the angular excitation frequencies at which local maxima were reached for the response amplitudes P ($\omega_{max,1} = 2.527$ rad s^{-1} and $\omega_{max,2} = 3.957$ rad s^{-1}) and for the response amplitudes D ($\omega_{max,1} = 2.583$ rad s^{-1} and $\omega_{max,2} = 3.962$ rad s^{-1}). In Fig. 7, it is important to point out the unusual shape of the response curve around the first local maximum. A large part of the response in this region falls within the unstable solution. This unstable area includes the local maximum of the response amplitude D with a value of $\omega_{max,1}$.

Based on the values shown in the previous graphs, the possible presence of a softening effect of the resonance curves can be inferred. This effect can be visually observed if we display all resonance curves in one image. To this end, Figs. 8 and 9 were created to show the response amplitudes P and D. The natural frequency of the linearized system of governing differential equations without the effect of damping and excitation force is added for comparison. Considering only small magnitudes of oscillations, we introduce the approximation $\sin\varphi \approx \varphi$ and $\cos\varphi \approx 1$. The modified system is given by the following equations:

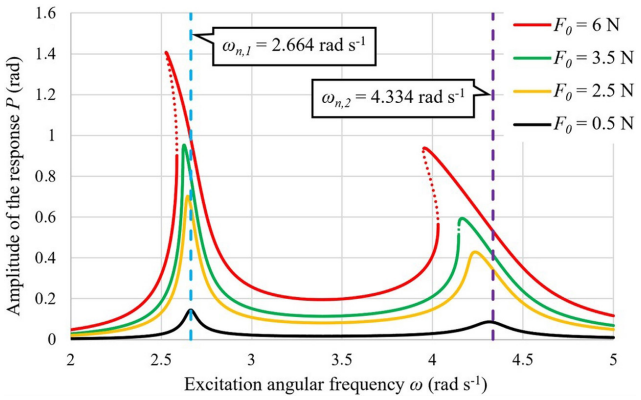

Fig. 8 Curves of response amplitudes P versus angular frequency of excitation ω for a system excited by a periodic force with multiple amplitudes . The solid line in these plots indicates the stable solution and the dotted line indicates the unstable solution. The dashed lines in the figure represent the natural angular frequencies and obtained from the linearized system. The values in the box specify their magnitudes

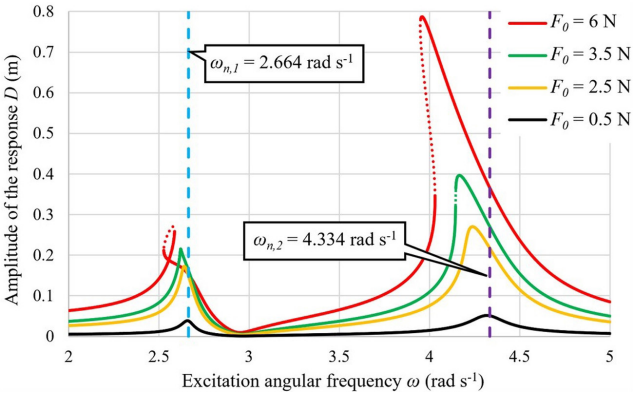

Fig. 9 Curves of response amplitudes D versus angular frequency of excitation ω for a system excited by a periodic force with multiple amplitudes . The solid line in these plots indicates the stable solution and the dotted line the unstable solution. The dashed lines in the figure represent the natural angular frequencies and obtained from the linearized system. The values in the box specify their magnitudes

$$\frac{7}{5}\rho\,\ddot{\varphi} + g\,\varphi + \ddot{u} = 0, \tag{56}$$

$$m\rho\,\ddot{\varphi} + (M+m)\ddot{u} + Ku = 0. \tag{57}$$

By numerical analysis in MATLAB software, the natural angular frequencies $\omega_{n,1} = 2.664$ rad s^{-1} and $\omega_{n,2} = 4.334$ rad s^{-1} were determined. The plots in Figs. 8 and 9 are calculated for four values of excitation force $F_0 = 0.5$, 2.5, 3.5 and 6 N. The smallest amplitude, which has not been analyzed in detail in this paper, is shown in order to illustrate the evolution of the softening effect.

5 Conclusions

The objective of the paper was to present one of the possible approaches for solving a system of nonlinear equations describing the motion of the ball vibrations absorber. The calculation process is illustrated through the example of a ball absorber placed in a bowl. The system of final equations is nonlinear, which can cause difficulties for classical numerical methods such as Newton's iterative method. These difficulties may not be apparent if the effect of nonlinearities is negligible. However, if the influence of non-linearities becomes significant, it is necessary to switch to other methods, such as the Continuation Method. In each step of the iteration, the Modified Secant Method is used to construct the Jacobi matrix and the resulting system of equations is solved using a built-in function of the mathematical software MATLAB called "*mldivide*". In each step of the calculation, the stability of the steady-state solution is validated using the Routh-Hurwitz criterion.

The functionality of the algorithm was further investigated using the example of a ball absorber whose response was

determined for three different values of the excitation force amplitude F_0 = 2.5, 3,5 and 6 N. It is assumed that an increase in the amplitude of the force will lead to a higher influence of the nonlinear behaviour of the system. The results of the calculations are presented in the form of a plot of the response component versus the angular excitation frequency. These simulations revealed a minor effect of nonlinearities when the value of the excitation force is equal to F_0 = 2.5 N. In other cases, the nonlinear character was evident, and unstable solutions were identified. Simulations with the amplitude of the excitation force F_0 = 3.5 N showed unstable regions only in the region of one of the two local peaks. For the highest simulated amplitude F_0 = 6 N, these regions were already present in both resonance domains. Furthermore, the presence of a softening effect was also observed in these plots for calculations with forces F_0 = 2.5, 3.5, and 6 N. The nature of stability of all solutions is done by analyzing the R-H conditions. For each calculated step a Routh matrix is constructed, and it is checked whether the values of the coefficients in the first column of this matrix have the same sign. If the assumption of identical sign holds, the solution is considered stable. Otherwise, it is an unstable solution.

In order to graphically represent the shift of the local maximum response values P and D, images that contain the results for all analyzed excitation force amplitudes are also created. Besides, an additional response curve with amplitude F_0 = 0.5 N and natural frequency of the linearized system is also added in the figures.

According to the results of the example, it can be seen that the presented algorithm is suitable for the calculation of linear systems or systems with small influence of nonlinearities, as well as for nonlinear systems.

However, it is useful to compare the results of the numerical simulations with the experimentally obtained data. There are plans to carry out experiments aimed at observing and assessing the motion of a ball situated on a semi-circular path with a specified radius. These experiments could potentially uncover additional novel insights into the behaviour of this kind of absorber.

Acknowledgement

The financial supports of the grant program financed by Ministry of Education, Youth and Sports of the Czech Republic through VSB–TUO SGS SP2023/059 and from the budget for conceptual development of science, research and innovations are highly acknowledged. The second author thanks to the Czech Foundation (GAČR) through project no. 22-13220S "Development of iterative algorithms for solving contact problems emerging in the analysis of steel structures bolt connections".

References

[1] Madarshahian, R., Caicedo, J. M., Zambrana, A. D. "Benchmark problem for human activity identification using floor vibrations", Expert Systems with Applications, 62, pp. 263–272, 2016. https://doi.org/10.1016/j.eswa.2016.06.027

[2] Jung, H.-J., Lee, S.-W. "The experimental validation of a new energy harvesting system based on the wake galloping phenomenon", Smart Materials and Structures, 20(5), 0055022, 2011. https://doi.org/10.1088/0964-1726/20/5/055022

[3] Kubo, Y., Modi, V. J., Kotsubo, C., Hayashida, K., Kato, K. "Suppression of wind-induced vibrations of tall structures through moving surface boundary-layer control", Journal of Wind Engineering and Industrial Aerodynamics, 61(2–3), pp. 181–194, 1996. https://doi.org/10.1016/0167-6105(96)00039-6

[4] Elias, S., Matsagar, V. "Research developments in vibration control of structures using passive tuned mass dampers", Annual Reviews in Control, 44, pp. 129–156, 2017. https://doi.org/10.1016/j.arcontrol.2017.09.015

[5] Chen, J., Georgakis, C. T. "Tuned rolling-ball dampers for vibration control in wind turbines", Journal of Sound and Vibration, 332(21), pp. 5271–5282, 2013. https://doi.org/10.1016/j.jsv.2013.05.019

[6] Pirner, M. "Actual behaviour of a ball vibration absorber", Journal of Wind Engineering and Industrial Aerodynamics, 90(8), pp. 987–1005, 2002. https://doi.org/10.1016/S0167-6105(02)00215-5

[7] Náprstek, J., Fischer, C., Pirner, M., Fischer, O. "Non-linear model of a ball vibration absorber", In: Papadrakakis, M., Fragiadakis, M., Plevris, V. (eds.) Computational Methods in Earthquake Engineering, Computational Methods in Applied Sciences, Springer, pp. 381–396, 2013 ISBN 978-94-007-6572-6 https://doi.org/10.1007/978-94-007-6573-3_18

[8] Matta, E. "Ball vibration absorbers with radially-increasing rolling friction", Mechanical Systems and Signal Processing, 132, pp. 353–379, 2019. https://doi.org/10.1016/j.ymssp.2019.06.033

[9] Sun, L., Li, S., Zhang, F. "Effect of self-resetting ball absorber on the mechanical properties of the fabricated structure and its influencing factors: Theory and Experimentation", Journal of Vibration Engineering and Technologies, 10(3), pp. 897–917, 2022. https://doi.org/10.1007/s42417-021-00418-3

[10] Papakonstantinou, J. M., Tapia, R. A. "Origin and evolution of the secant method in one dimension", The American Mathematical Monthly, 120(6), pp. 500–517, 2013. https://doi.org/10.4169/amer.math.monthly.120.06.500

[11] Juhari, J. "On the modification of newton-secant method in solving nonlinear equations for multiple zeros of trigonometric function", CAUCHY – Jurnal Matematika Murni dan Aplikasi, 7(1), pp. 84–96, 2021. https://doi.org/10.18860/ca.v7i1.12934

[12] Vanroose, W., Broeckhove, J., Kłosiewicz, P. "Tracing the parameter dependence of quantum resonances with numerical continuation", Journal of Physics B: Atomic, Molecular and Optical Physics, 42, 044002, 2009. https://doi.org/10.1088/0953-4075/42/4/044002

[13] Willers, C., Thiele, U., Archer, A. J., Lloyd, D. J. B., Kamps, O. "Adaptive stochastic continuation with a modified lifting procedure applied to complex systems", Physical Review E, 102, 032210, 2020. https://doi.org/10.1103/PhysRevE.102.032210

[14] Ficken, F. A. "The continuation method for functional equations", Communications on Pure and Applied Mathematics, 4(4), pp. 435–456, 1951. https://doi.org/10.1002/cpa.3160040405

[15] Allgower, L. A., Georg, K. "Introduction to numerical continuation methods", Society for Industrial and Applied Mathematics, 1987. ISBN 978-0898715446

[16] Rheinboldt, W. C. "Numerical analysis of continuation methods for nonlinear structural problems", Computers and Structures, 13(1–3), pp. 103–113, 1981. https://doi.org/10.1016/0045-7949(81)90114-0

[17] Gatti, G. "Fundamental insight on the performance of a nonlinear tuned mass damper", Meccanica, 53(1–2), pp. 111–123, 2018. https://doi.org/10.1007/s11012-017-0723-0

[18] Apte, Y. S. "Routh-Hurwitz stability criterion and its equivalents", IEE-IERE Proceedings – India, 7(4), pp. 149–154, 1969. https://doi.org/10.1049/iipi.1969.0039

[19] Minguzzi, E., "Rayleigh's dissipation function at work", European Journal of Physics, 36(3), 035014, 2015. https://doi.org/10.1088/0143-0807/36/3/035014

[20] Quin, T., RAI, S. "Variation of parameters in differential equations (A variation in making sense of variation of parameters)", PRIMUS, 23(1), pp. 25–44, 2012. https://doi.org/10.1080/10511970.2012.694016

[21] Boyce, E. W., DiPrima, R. C. "Elementary differential equations and boundary value problems", John Wiley and Sons, 2009. ISBN 978-0-470-38334-6 [online] Available at: https://s2pnd-matematika.fkip.unpatti.ac.id/wp-content/uploads/2019/03/Elementary-Diffrential-Aquation-and-Boundary-Value-Problem-Boyce-DiPrima.pdf [Accessed: 10 December 2024]

[22] Bogoliubov, N. N., Mitropolsky, Y. A. "Asymptotic methods in the theory of nonlinear oscillations", Gordon and Breach Science Publishers Ltd., 1961. ISBN 978-0677200514

[23] Yan, Z., Dai, H., Wang, Q., Atluri, S. N. "Harmonic balance methods: A review and recent developments", Computer Modeling in Engineering and Sciences, 137(2), pp. 1419–1459, 2023. https://doi.org/10.32604/cmes.2023.028198

[24] Kawulok, M., Pospisil, S., Freiherrova, N., Juracka, D. "Numerical simulation of a planar model of a ball absorber in a spherical dish", Periodica Polytechnica Civil Engineering, 67(3), pp. 855–866, 2023. https://doi.org/10.3311/PPci.21725

[25] Math. Graphics. Programming. "Matlab, (R2020a)", MathWorks, [computer program] Available at: https://www.mathworks.com/products/matlab.html?s_tid=hp_ff_p_matlab [Accessed: 13 December 2023]

[26] MathWorks: Help Center "Mldivide, \: Solve systems of linear equations Ax = B for x", [online] Available at: https://www.mathworks.com/help/matlab/ref/mldivide.html [Accessed: 13 December 2023]